ISSN 2347-3487

Effect of rapid solidification on microstructure, creep resistance and thermal properties of Sn-10 wt.% Sb- 3 wt.% X (X= In, Ag, Bi and Zn) lead-free solder alloys

Rizk Mostafa Shalaby*

Metal Physics Laboratory, Physics Department, Faculty of Science, Mansoura University, Mansoura, B.O.Box: 35516, Mansoura, Egypt.

*Corresponding author: doctorrizk2@yahoo.co.uk

Tel.: +2- 01150645223, +2- 01062507736

Abstract

The harmful effects of lead on the environment and human health, coupled with the threat of legislation, have prompted a serious search of lead-free solders for electronic packaging applications. The melt-spinning processes of ternary Sn-10 wt.%Sb-3 wt.%X (X=In, Ag, Bi and Zn) were analyzed using x-ray diffractometer (XRD), scanning electron microscopy (SEM), differential scanning calorimetry (DSC) and Vickers hardness tester (H_V). The investigation showed that, the addition of a small amount of the third element enhances the ductility of the Sn–10 wt. % Sb lead-free solder due to the formation of a fine, homogeneous ternary microstructure. It is concluded that, the addition of 3.0 wt% Ag improves the grain size of the ternary microstructure. The fine precipitates from SnSb intermetallic compound suppresses the coarsening of the ternary structure and thus enhances solder ductility. Structural and microstructural analysis revealed that the origin of change in mechanical behaviors was due to refined beta-Sn grains and formation of intermetallic compounds (IMCs) SnSb, $InSn_{19}$, β-In_3Sn and Ag_3Sn. The results indicated that the melting point of Sn-10Sb-3 wt.% Ag and Sn-10 wt.%Sb- 3 wt.% Zn alloys reduced to 230 and 240 ˚C respectively. In particular, the zinc addition at 3 wt.% is the most effective in improving solder ductility and good creep resistance correlated to a fine grain size and complete soluble of SnSb IMC particles in the β-Sn matrix.

Keywords

Rapid solidification; Intermetallic compounds; Mechanical properties; Creep resistance; Thermal properties.

Council for Innovative Research

Peer Review Research Publishing System

Journal: JOURNAL OF ADVANCES IN PHYSICS

Vol.9, No.1

www.cirjap.com, japeditor@gmail.com

ISSN 2347-3487

1. Introduction

There has been considerable scientific and technological interest in using rapid solidification processing with cooling rates during solidification of $>10^5$ k/s to produce new structures and improved properties in a variety of metallic alloys. It is well known that the use of solders has become indispensable for the interconnection and packaging of virtually all electronic devices and circuits. In general, the 95Pb-5Sn solder with a melting temperature of 308-312 ˚C is used for high temperature applications in step soldering. However, due to environmental issues, the use of Pb is restricted and new Pb-free high temperature solder alloys are required. Antimony has been used as the alloying element in the Sn based system as suitable substitutes for Sn-Pb solder alloys. The addition of Sb element to Sn has the influence on strength and hardness to the alloy. Formations of SnSb intermetallic phase have a cubic structure with a high hardness. Tin – Antimony alloys are modified have been studied [1]. The obtained data by slow cooling compared with the high cooling, affects the microstructure and properties of tin-antimony alloys. They found that refined structure and therefore, gives enhances mechanical properties. Several studies on tin-antimony solder alloys have been reported, covering their solidification behavior [2], interfacial reactions on substrates [3-4], and mechanical properties [5- 8]. Effect of In element on electrical, thermal and mechanical properties of lead free Sn-Sb solder alloys rapidly solidified from melt [9]. The results showed that new intermetallic compound In_3Sn and supersaturated solid solution were produced by melt spun technique. Also, reported that a minor addition of indium significantly decreases the melting points of Sn-10Sb alloy. The Sn-5Sb system is an alloy with a high melting point that has been developed to replace the widely used Sn-37Pb solders [10]. Hence, an additional Sn-10Sb alloy with a higher amount of Sb was chosen as another candidate together with Sn-5Sb. The Sb quantity cannot be increased, since a high quantity of Sb causes multiple agglutinations of the SnSb crystals in the matrix. Appropriate quantity of Sb is about 12 wt. %. Effects of Sb on sliding wear resistance of white metal have been studied by Ishehira [11]. Wear resistance is not affected by the amount of antimony within a range 5-18 wt.% ; however the resistance is decreased at the higher amount of antimony. Mechanical and thermal properties of bearing metals improved by adding elements such as Bi, Ag, In and Zn. Minor addition of Zn element causes refined grain size Effect of heating and solidification rate on hardness and microstructure of tin based white metals have been studied by Goudarzi et al [12]. They show that the higher cooling decreases growth and formation of SnSb crystals and enhances hardness. Physical properties of the rapidly cooling lead-free Sn-10Sb-Cu-Zn alloys were studied by [13]. The results indicated that hardness, Elastic moduli (E) and electrical resistivity are increased by increasing the zinc content. Sn-Sb alloys are considered of great potential [14]. Most works, which have been carried out in this field were mainly focused on the mechanical properties of the bulk solders [15, 16], such as the tensile property [17] and creep property [18, 19]. The mechanical and electrical properties of solders are important because solder joints connect mechanically and electrically integrated circuit chips with the substrate. In this study the Sn-10 wt.% Sb-3 wt.% X (X = In, Bi, Ag, and Zn) alloys were selected to replace Sn-37Pb for step soldering used in advanced packaging applications and investigated in terms of microstructure, mechanical and thermal properties.

2. Experimental procedures

2.1. Materials

The Sn-based solder melt- spun alloys (Sn-10 wt.%Sb- wt.%3Ag, Sn-1 wt.%0Sb-3 wt.%Bi, Sn-10 wt.%Sb-3 wt.%In and Sn-10 wt.%Sb-3 wt.%Zn were prepared from high-purity grade metals (purity higher than 99.9 %). Table 1 shows the chemical compositions of elements. Four alloys of compositions have been produced by a single copper roller melt-spun technique. Required quantities of the used metals were weighed out and melted in a porcelain crucible. After the alloys were molten, the melt was thoroughly agitated to effect homogenization. The casting was done in air at a melt temperature of 600 °C. The speed of copper wheel was fixed at 2900 rpm; which corresponds to a linear speed of 30.4 m/s. The resulting alloys have long ribbons from of about 100 µm in thickness and 1 cm width.

Table 1:

Chemical compositions of the produced alloys (wt.%) with different additions.

Solder	Sn wt.%	Sb wt.%	In wt.%	Ag wt.%	Bi wt.%	Zn wt.%
Sn-10 wt.%Sb-3 wt.%In	87	10	3			
Sn-10 wt.%Sb-3 wt.% Ag	87	10		3		
Sn-10 wt.%Sb-3 wt.%Bi	87	10			3	
Sn-10 wt.%Sb-3 wt.%Zn	87	10				3

ISSN 2347-3487

2.2. Characterization methods

X-ray diffraction (XRD) measurements were performed to identify the phases formed in the produced melt-spun alloys. The microstructure analysis was carried out on a scanning electron microscopy (SEM) of type (JEOL JSM-6510LV, Japan) operate at 30 KV with high resolution 3 nm. Differential Scanning Calorimetry (DSC) was used to measure thermal properties and melting points with a heating rate 10 k/min of the four Sn-based solder melt-spun alloys in the temperature range from 20 °C to 450 °C. Vickers hardness Hv tests were performed at a load 10 g in order to examine the mechanical properties. The Vickers hardness number (Hv) is measured using the FM-7 microhardness tester, Japan. The mechanical properties of the produced melt-spun alloys were examined by a dynamic resonance technique [20]. The electrical resistivity was measured by double bridge method at room temperature. Creep measurements as described elsewhere [21] and hardness measurements were also carried out using a Vickers hardness technique using a fixed load of 0.49 N.

3. Results and discussion

3.1 Phase identification

The X-ray diffraction patterns for all produced melt-spun alloys Sn-10 wt.%Sb-3 wt.%X (X= In, Ag, Bi and Zn) showed several peaks as shown in Fig.1. The peaks of the XRD patterns given in Fig.1 (a-d) show that the diffracted X-rays come from ordered atomic orientations arranged in numerous sets of parallel planes in the crystal [22]. All measured physical properties affected by small amounts of alloying elements and changed its structural properties. X-ray diffraction patterns indicated that the Sn-10 wt.%Sb-3 wt.%X (X= In, Ag, Bi) alloys have body centered tetragonal of Sn matrix, in addition to more intermetallic compounds, such as SnSb, β-In_3Sn, $InSn_{19}$ precipitates in the Sn matrix. These phases do not exist in diffraction pattern of the as conventional alloy. This result indicates that rapid solidification effects are inherent in conventional method. The structure of Sn-10 wt.%Sb-3 wt.%In melt-spun alloy Fig.1a contains SnSb, $InSn_{19}$, and β-In_3Sn (The In_3Sn compound has β-tetragonal structure) intermetallic phases embedded in the Sn matrix which is not normally obtained under equilibrium conditions. For Sn-10 wt.%Sb-3 wt.%Ag alloy Fig.1b, Ag_3Sn was formed in addition to the formation of SbSn. For Sn-10 wt.%Sb-3 wt.%Bi Fig.1c shows that presence of SnSb and β-Sn phases. On the other side, the structure of Sn-10 wt.%Sb-3 wt.%Zn alloy contains β-Sn phase only, Fig.1d there are not any intermetallic phases embedded in the tin matrix. This result may be desirable for solder because an intermetallic compound SnSb disappear from the matrix. The variations of the volume of the unit cell and the measured density have an opposite trend, in agreement with the equation [23]: $\sum A=\delta v/1.6602$. Where $\sum A$ is the sum of the atomic weight in the unit cell, δ is measured density in g/cm^3 and v is the volume of the unit cell in nm^3. The value of the measured density for pure Sn rapidly solidified is 7 g/cm^3, when this value is substituted in above equation, it gives 456.5 for $\sum A$. By dividing the value of $\sum A$ by the atomic weight of Sn (118.69), it gives the number of atoms per unit cell less than 4, which must be 4 for β-Sn. Therefore, some of the atoms may be missing from a certain fraction of these lattice sites that they would be expected to occupy. The grain size is determined from the x-ray diffraction pattern by using Scherrer's equation $D_{hkl}=0.9\lambda/\beta_{hkl}\cos\theta$, where D_{hkl} is the grain size, λis the wavelength of CuK_α = 1.54056 A, θ is the reflection angle and β_{hkl} is the full width at half maximum (FWHM) [23]. The details of the XRD analysis are shown in Table 2.

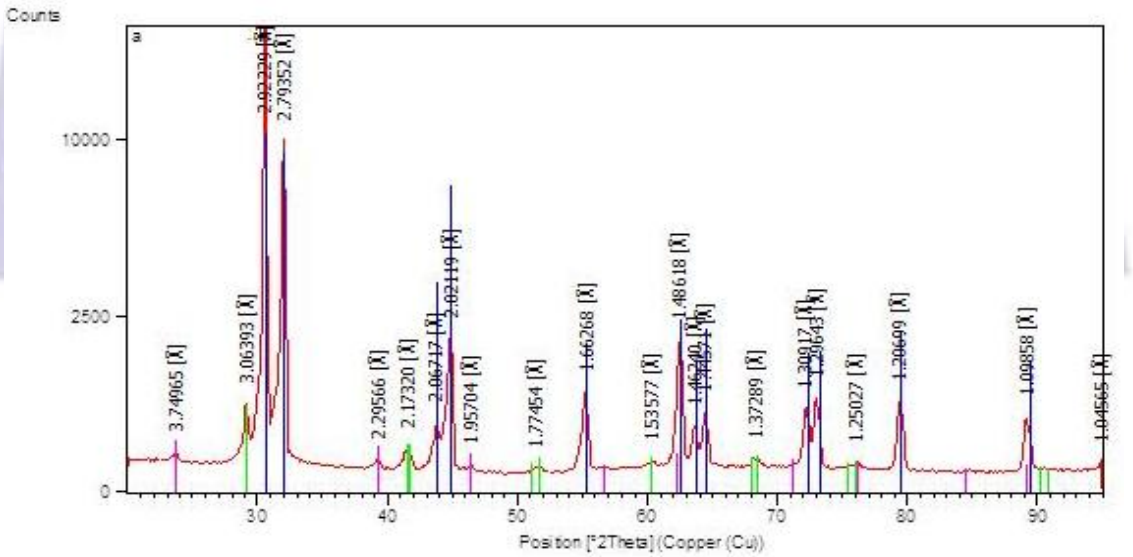

ISSN 2347-3487

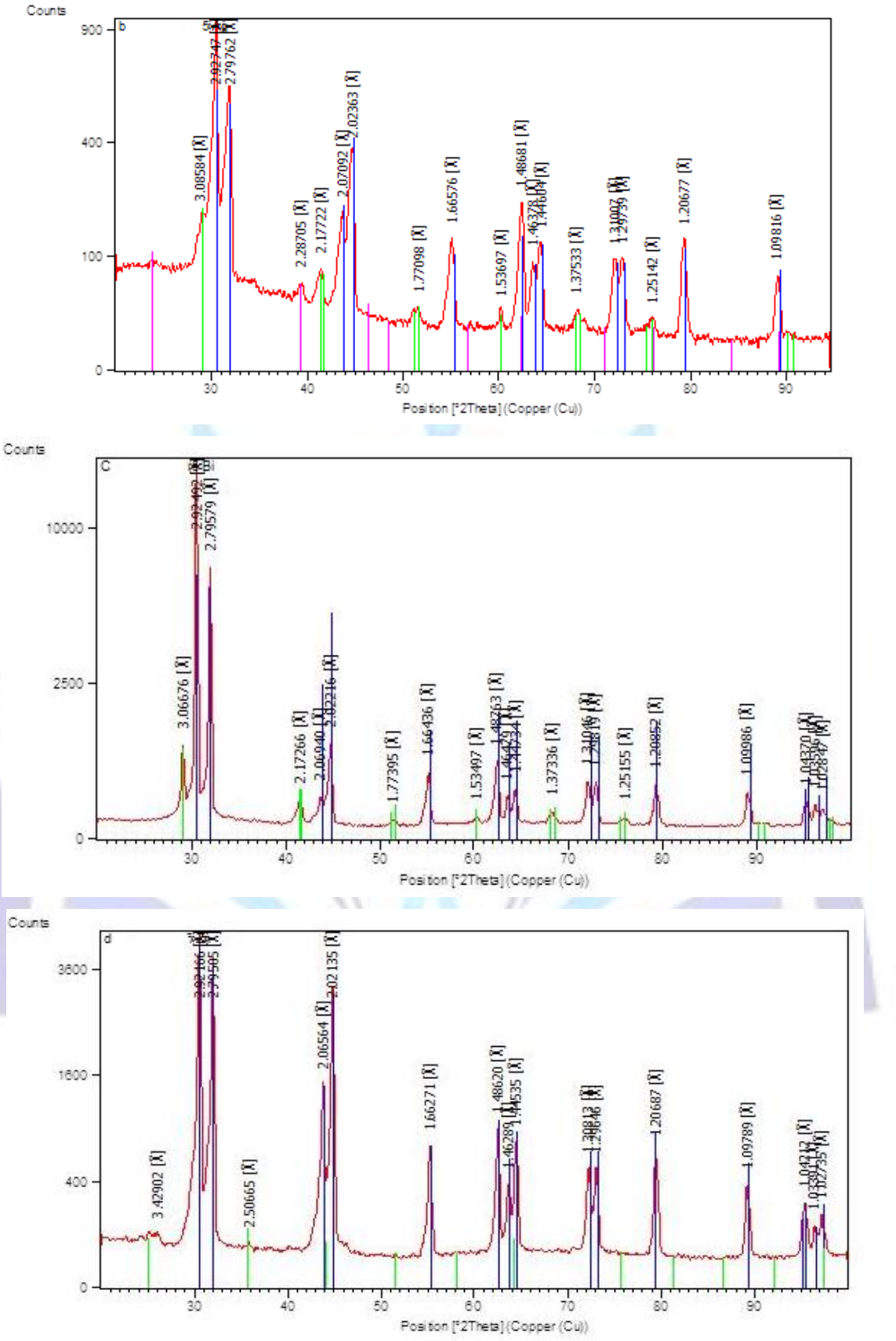

Fig.1 Detail of the phases and constituents obtained by XRD for: (a) Sn-10 wt.% Sb-3 wt.% In, (b) Sn-10 wt.%Sb-3 wt.% Ag, (c) Sn-10 wt.%Sb-3 wt.% Bi, and (d) Sn-10 wt.%Sb-3 wt.% Zn.

ISSN 2347-3487

Table 2

Detail of the phases and lattice parameters obtained by XRD.

Solder	Phase designation	Crystal system	Grain size nm	Lattice parameter			No. of atoms per unit cell
				a(Å)	c (Å)	c/a	
Sn-10 wt.%Sb -3 wt.%In	β-Sn SbSn $InSn_{19}$ $β-In_3Sn$	Body centered tetragonal Rhombohedral Tetragonal Tetragonal	330.32	5.84458	3.1803	0.54414	3.52
Sn-10 wt.%Sb -3 wt.%Ag	β-Sn SbSn Ag_3Sn	Body centered tetragonal Rhombohedral Orthorhombic	280.15	5.85494	3.18469	0.54393	3.22
Sn-10 wt.%Sb -3 wt.%Bi	β-Sn SbSn	Body centered tetragonal Rhombohedral	385.42	5.84984	3.18282	0.54408	2.95
Sn-10 wt.%Sb -3 wt.%Zn	β-Sn	Body centered tetragonal	490.24	5.84332	3.18279	0.54468	3.70

3.2 Microstructure

In order to understand the microstructure evolution of Sn-10Sb-3X (X= In, Ag, Bi and Zn) melt spun alloys during rapid solidification, the samples were examined by SEM. As-cast microstructures of Sn-10Sb-3X (X= In, Ag, Bi and Zn) are shown in Fig.2 The microstructure of Sn-10Sb-3X (X= In, Ag, Bi and Zn) melt spun alloys appears as Sn-matrix in addition to some fine precipitations of IMCs as detected from x-ray diffraction analysis. With trace amount of In, Ag, Bi Zn at 3 wt.% addition the grain size are much finer. Therefore, the intermetallic compounds are uniform distribution in β-Sn. As we know that the existences of bulk intermetallics are harmful to the mechanical performance of the solder. It is noticed that the intermetallics are thin and more refined. Fig. 2(d) for 3 wt.% Zn, appears the microstructure without any intermetallics. Also, It was reported that In, Ag, Bi and Zn additions at 3 wt.% modified the the β-Sn grains. The finer and more homogeneous microstructure can have a preferable effect on the mechanical performance of the produced solder.

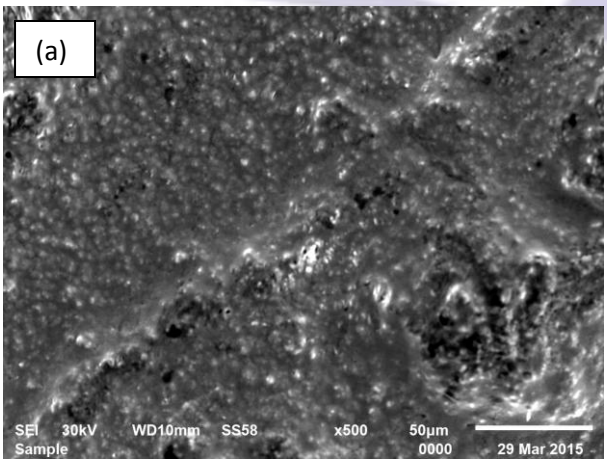

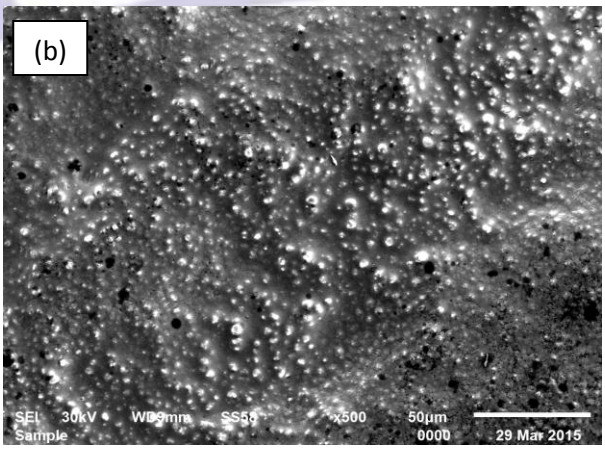

ISSN 2347-3487

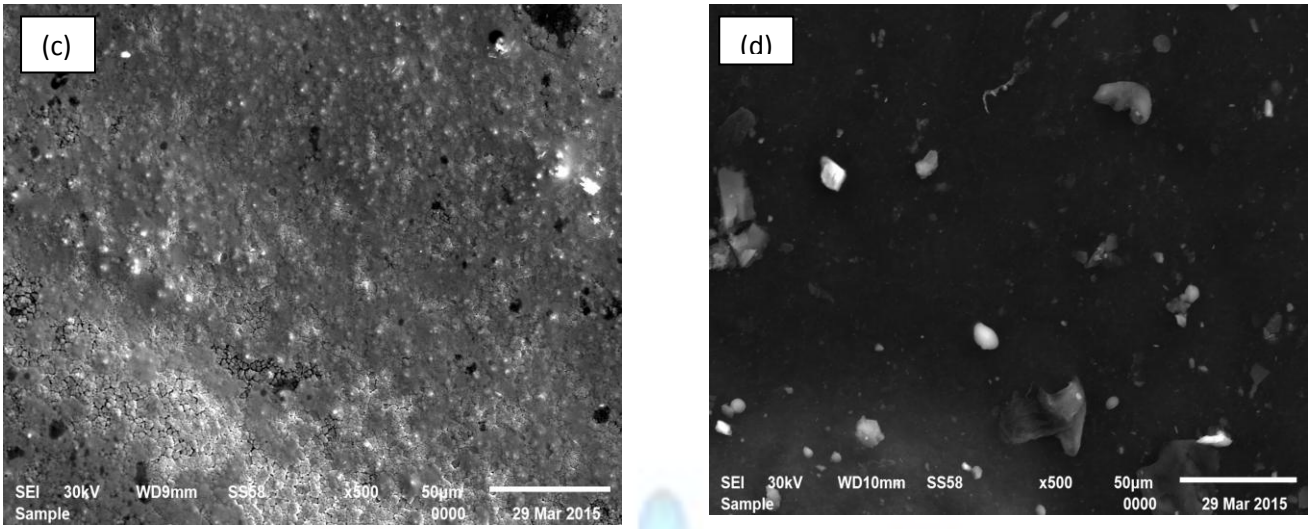

Fig.2: Detail of the phases and constituents obtained by SEM for: (a) Sn-10 wt.% Sb-3 wt.% In, (b) Sn-10 wt.%Sb-3 wt.% Ag, (c) Sn-10 wt.%Sb-3 wt.% Bi, and (d) Sn-10 wt.%Sb-3 wt.% Zn.

3.3 Melting behaviors of Sn-10Sb-3X(X= In, Ag, Bi and Zn) lead free solders

Sn-10Sb-3X (X=In, Ag, Bi and Zn) solder alloys with heating rate 10 K/min investigated by DSC as shown in Fig.3. The melting points for each alloy, i.e., temperature of the solidus (T_s) and liquidus (T_l) are shown in Table 3. As shown in Fig.3 there is no any phase transformation observed in the temperature range from 20 °C to 450 °C excluding the melting point which is indicated by the exothermic peak of melting for all produced melt-spun alloys. From this figure the melting point T_m, and pasty range (temperature range between solidus and liquidus points according to DSC) of these alloys are calculated and presented in Table 3. Table 3 shows that the melting temperature decreases with Ag and Zn additions at 3 wt.%. Silver and zinc addition at 3.wt% moved the peak to a lower temperature. The addition of Bi at 3 wt.% has much more significant effect than In, Zn and Ag addition, especially on the liquidus temperature. This is attributed to In element has a lower melting point compared with melting points of other used elements. The melting temperature reaches about 230 °C and 240 ˚C at 3 wt.% Ag and Zn respectively. Therefore the Sn-10Sb-3.wt.% Ag and Sn-10 wt.% Sb-3 wt.% Zn have lowest melting points and suitable for soldering applications instead of common Sn-Pb solder alloy.

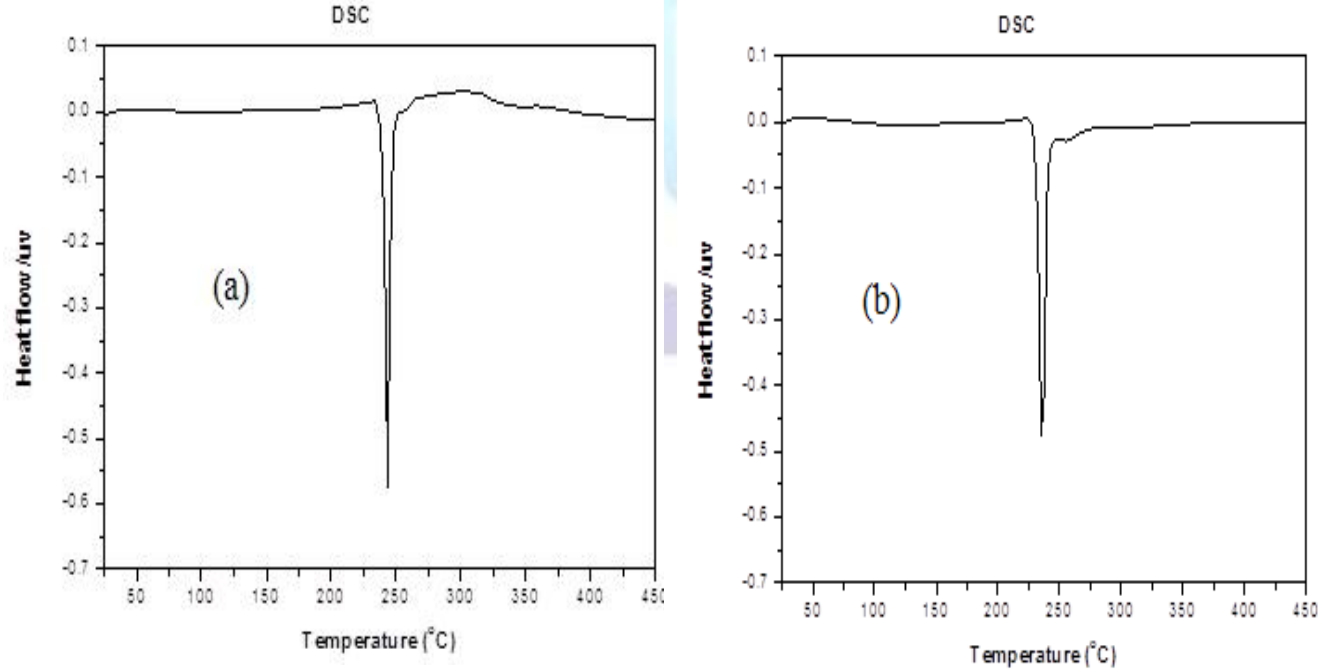

ISSN 2347-3487

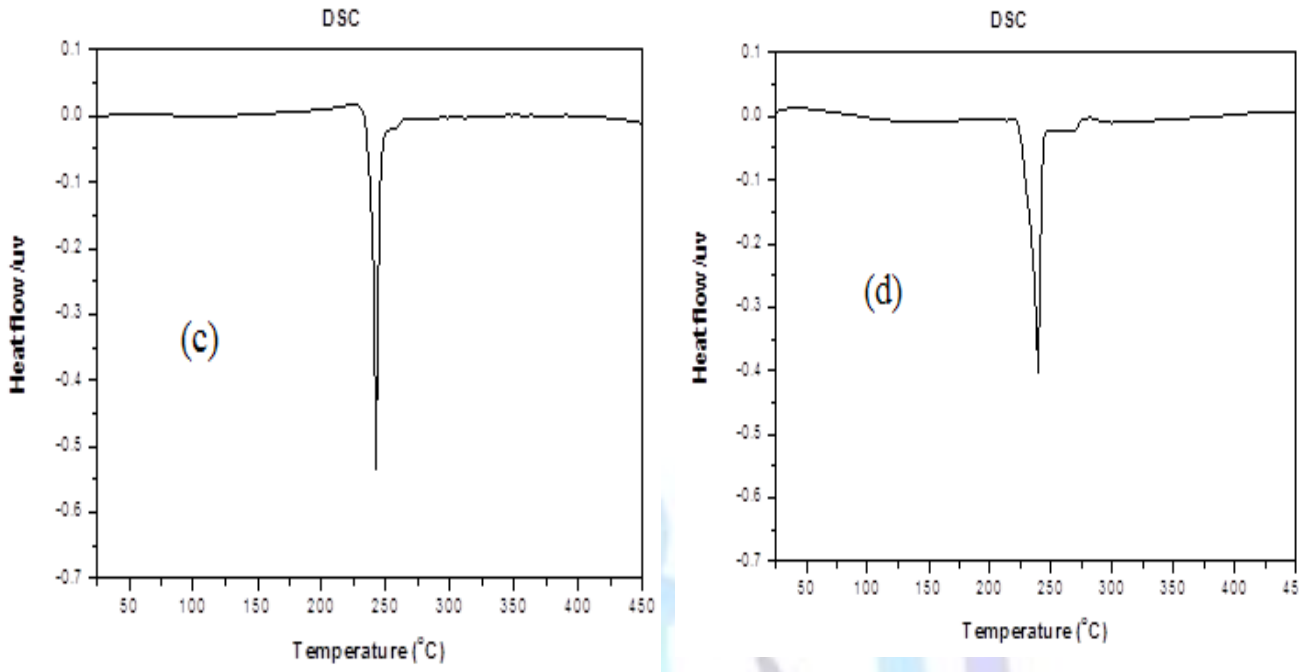

Fig.3 Thermal properties and melting points by DSC of produced ribbons (a) Sn- wt.% Sb-3 wt.% In, (b) Sn-10 wt.% Sb-3 wt.% Ag, (c) Sn-10 wt.% Sb-3 wt.% Bi, and (d) Sn- 10 wt.% Sb-3 wt.% Zn .

Table 3

Thermal analysis of all produced melt spun alloys

Solder	Solidus temperature (T_s) °C	Liquidus temperature (T_l) °C	Melting point (T_m) °C	Pasty range (liquidus – solidus temperature) °C
Sn-10 wt.%Sb-3 wt.%In	237.5	250	245	12.5
Sn-10 wt.%Sb-3 wt.%Ag	227.0	250	230	23.0
Sn-10 wt.%Sb-3 wt.%Bi	237.0	252	247	15.0
Sn-10 wt.%Sb-3 wt.%Zn	225.0	250	240	25.0

3.4 Microhardness of the solder alloys doped with small additions

The microhardness test results of the Sn-10Sb-3X (X=In, Ag, Bi and Zn) melt spun alloys are shown in Fig4. The microhardness properties are basically related to the crystal structure of the material. Consequently, microhardness studies have been applied in order to understand the plastically of the grains [24]. Table 4 shows the Vickers microhardness (Hv) of melt-spun Sn-10Sb-3 X (X= In, Ag, Bi and Zn) solder alloys. The hardness increased by adding Zn to melt-spun Sn-10Sb based solder alloy, this is due to soluble of hard phase within a soft matrix β-Sn. Also, may be attributed to the hard bonding force between Sn-Zn atoms than that between Sn-Sb phases [24]. The experimental determination involves the measurement of the time and load dependence of hardness in addition to the effect of small addition in binary Sn-10Sb alloy. Figure 4 shows the variation of microhardness Hv with dwell time (5-99 s) for different applied load (0.098 -2.94 N). It is found that the hardness decreases with increasing applied load for all Sn-10Sb-3X (X=In, Ag, Bi and Zn) systems. It can be concluded that the Sn-10Sb-3In and Sn-10Sb-3Zn systems significantly strength and delay the fracture up to 2.94 N, 99 s. This is may be due to the presence of IMCs, SnSb, $InSn_{19}$ and β-In_3Sn for Sn-10Sb-3In alloy but may be due to the interfacial reactions in the Sn/Sb, Sb/Zn or Sn/Zn couples for Sn-10Sb-3Zn alloy. Since no any intermetallics present in the Sn-10Sb-3Zn system, the Sn-Sb-Zn alloy exhibits excellent ductility at room temperature. It also concluded that for Sn-10Sb-3Ag and Sn-10Sb-3Bi the fracture happens at 0.98 N, 99 s and 1.96 N, 99

s respectively. This behavior can be explained in terms of the alloy structure and resulting properties. Addition of antimony leads to presence of SbSn, as a hard inclusions in the Sn matrix. The grains of SnSb may be act as crack initiation sites and eventually lead to fracture. Therefore, the high strength of Sb content imparts more strength for microelectronics applications.

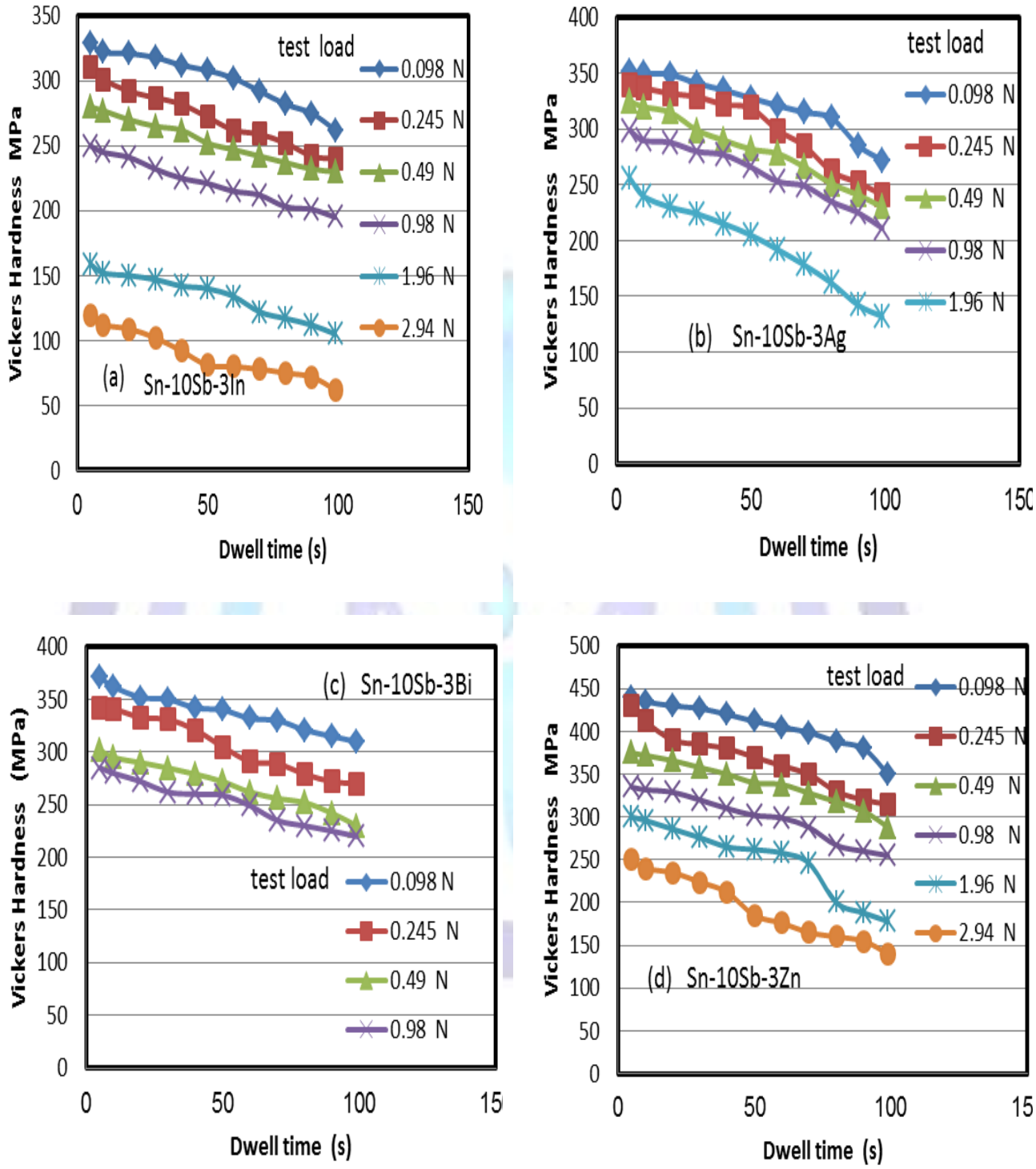

Fig.4: Variation of Vickers hardness (H_v) with dwell time.

ISSN 2347-3487

Table 4

The Vickers hardness number values of Sn-10 wt.%Sb-3 wt.%X (X=In, Ag, Bi and Zn) solder alloys.

Solder	Hv MPa (5 sec, 10 gf)	σ_y Mpa
Sn-10 wt.%Sb-3 wt.%In	328.74	109.58
Sn-10 wt.%Sb-3 wt.%Ag	351.54	117.18
Sn-10 wt.%Sb-3 wt.%Bi	371.24	123.74
Sn-10 wt.%Sb-3 wt.%Zn	240.15	80.050

3.5 Mechanical Properties

Mechanical properties of Sn-10 wt.%Sb-3 wt.%X (X=In, Ag, Bi and Zn) solders were studied. Table 5 shows the results of the mechanical properties of all produced melt-spun alloys. As shown in Table 5, the Elastic moduli and Lam's constant are increases to the higher value of 67.54 GPa at 3 wt. % Ag. This is may be presence of different IMCs for this alloy as indicated by XRD. Bulk moduli (B), Shear moduli (G), and Lame's constant (λ) calculated using equations;

$$B = \frac{E}{3(1-2\nu)}, \qquad G = \frac{E}{2(1+\nu)} \qquad and \qquad \lambda = \frac{\nu E}{(1+\nu)(1-2\nu)}$$

Theoretical cohesive strength (δ_t), The tensile fracture strength (σ_f), tensile fracture strain ($\varepsilon_{t,f}=\sigma_f/E$), and compressive yield strain($\varepsilon_{c,y}=H_v/3E$) are shown in Table 5. It is found that the calculated values of compressive yield strength, theoretical cohesive strength, tensile fracture strain and tensile fracture strength are increasing with Ag addition at 3 wt.%. This result may be attributed to hard inclusions from IMCs precipitates in the Sn matrix.

Table 5:

Elastic moduli and mechanical properties of produced melt-spun Sn-10 wt.% Sb-3 wt.% X (X=In, Ag, Bi and Zn) solder alloys.

Solder	Young's Modulus E GPa	Shear modulus G GPa	Bulk modulus B GPa	Lame's constant λ GPa	σ_t GPa	σ_f GPa	$\varepsilon_{t,f}$	$\varepsilon_{c,y}$ 10^{-3}	Poisson's ratio
Sn-10 wt.%Sb -3 wt.%In	66.36	24.397	79.00	62.7350	10.489	20.978	0.361	1.651	0.36000
Sn-10 wt.%Sb -3 wt.%Ag	67.54	24.840	80.12	63.5579	10.677	21.355	0.316	1.734	0.35950
Sn-10 wt.%Sb -3 wt.%Bi	63.53	23.430	74.69	59.100	10.390	20.781	0.317	1.947	0.35825
Sn-10 wt.%Sb -3 wt.%Zn	60.25	22.170	71.00	56.3100	10.790	21.580	0.316	2.430	0.35875

ISSN 2347-3487

3.6 Micro-creep

Variation of Hv versus indentation time is shown in Fig.4. Vickers hardness Hv decreases with dwell time. The Vickers hardness determined from equation, Hv = 0.102 F/S MPa, where F is the acting load in N, and S is the surface area of the indentation mm^2. If acting force is fixed, the Hv decreases due to the increase of area. The area increasing (strain) here is considered as the fractional change in area and is given by equation; strain (ε) = $\Delta S/S_0$, where, ΔS is the increase in area and S_0 is the original area taken at the lowest of the dwell time. From Hv above equation and from Fig.4, the strain can be calculated with the indentation time since the applied load was fixed for all the experiments [21]. Fig.5 shows the relation between the ε of Sn-10Sb-3X (X= In, Ag, Bi and Zn) melt spun alloys versus dwell time in time interval from 0 to 90 s using a constant load of 0.0.098 N. The first stage records a fast increase of strain with time of the indentation starts from the beginning up to 40 % of the total indentation time. The second stage represents a steady state region in which the strain increases by lower rates for all alloys. The creep resistance of the Sn-10Sb alloy has been enhanced with the 3 wt.% Zn . As shown in Fig.5, the creep resistance reaches a maximum at 3 wt.% Zn and then decrease when In, Ag and Bi are added. It is believed there are two major strengthening mechanisms from the stiff metal particles. One comes from the pinning of the dislocation movement through effective particle dislocation interactions. Secondly, large grain size for 3 wt.% Zn promotes diffusional creep , grain boundary sliding and decrease the dislocations movements, adversely affecting creep resistance especially at lower load.

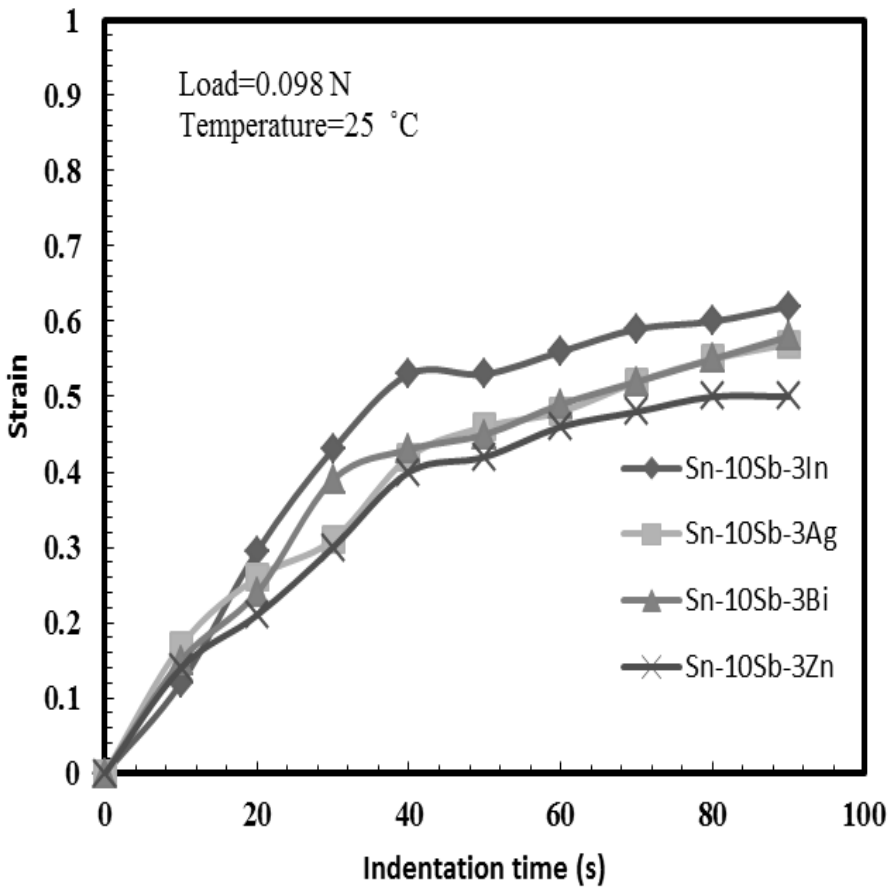

Figure 5: Micro-creep curves of Sn-10 wt.% Sb-3 wt.% X (X=In, Ag, Bi and Zn) melt spun alloys.

3.7 Electrical resistivity

In microelectronic industries the electrical resistivity of the solder interconnects should be thinner that it does not affect the functionality of the electric circuit. The electrical resistivity (ρ) of melt-spun lead free solder alloys are measured at room temperature as shown in Table 6. As shown in Table 6 the electrical resistivity increases after addition In at 3 wt. %. This result may be attributed to the formation of SbSn and In_3Sn IMCs phases and effect of rapid cooling [25] which acts hard inclusions in the soft matrix. On the other side, the high resistivity of Sn-10Sb-3Bi when compared with that three another alloys are related to increases scattering of the conduction electrons due to a random atomic arrangement. As crystalline defects serve as scattering centers for the conduction electrons in metals, increasing their number increases the resistivity. The decrease in the resistivity may be attributed to the various factors facilitate the free transfer of valence electrons through the lattice at 3 wt.% Zn . Since no intermetallic compounds form in the Sn-10Sb-3Zn system, leads to decreasing in electrical resistivity and this conclusion correlate with the mechanical properties. This result recommended for electronics applications as a solder alloy.

ISSN 2347-3487

Table 6

The electrical resistivity, ρ, values of rapidly solidified Sn-10 wt.% Sb-3 wt.% X (X= In, Ag, Bi and Zn) solder alloys at room temperature.

Solder	Electrical resistivity (ρ) at room temperature (10^{-6} Ω.cm)
Sn-10 wt.%Sb-3 wt.%In	42.35
Sn-10 wt.%Sb-3 wt.%Ag	40.55
Sn-10 wt.%Sb-3 wt.%Bi	36.50
Sn-10 wt.%Sb-3 wt.%Zn	32.23

Conclusions

Four lead free solder alloys Sn-10Sb-3X (X=In, Ag, Bi and Zn) were prepared by melt-spun process rapidly solidified from melt. The results are summarized in the following points:

1- The results showed that In, Ag, Bi and Zn are completely dissolved in matrix and increased the solubility of due to rapid solidification process.

2- As observed by structure and microstructural analysis, the typical structure of Sn-10Sb-3X (X=In, Ag, Bi and Zn) alloys are composed of β-Sn phase and mixed granules of SnSb, β-In_3Sn, $InSn_{19}$ and Ag_3Sn of IMCs. There aren't any intermetallics for the Sn-10Sb-3Zn system; therefore, Sn-Sb-Zn alloy exhibits excellent ductility at room temperature.

3- Because of the defects and lattice distortion occurs, then the number of atoms per unit cell in this study are non-integer numbers compared with the number of atom per unit cell of Sn phase = 4.

4- It is found that for Zn addition, the electrical resistivity value of Sn-10Sb-3Zn melt-spun alloy decreases, because of the scattering centers for the electrons decrease which leads to increase orderly atomic arrangement, so a net increase in the conductivity occurs.

5- The results indicated that the melting point of Sn-10Sb-3 wt.% Ag and Sn-10 wt.%Sb- 3 wt.% Zn alloys reduced to 230 and 240 ˚C respectively. The pasty range (difference between solidus and liquidus temperature) reduced to 12.5 and 15 ˚C for Sn-10 wt.% Sb- 3 wt.% In and Sn-10 wt.% Sb- 3 wt.% Bi . The good creep resistance of Sn-10 wt.% Sb-3 wt.% Zn lead-free solder correlated to a fine β-Sn grains size and complete soluble of SnSb IMC particles in the β-Sn matrix.

6- Creep measured by Vickers hardness tester is a suitable for this type of alloys since it is non-destructive method and useful for produced alloys.

7- The ternary Sn-10Sb-3Zn lead-free solder has the most suitable properties required for advanced packaging applications as a replacement of Sn-Pb eutectic alloy.

Acknowledgement I express my deep gratitude and appreciation to Professor M.Kamal, Head of Metal Physics Group, Physics Department, Faculty of Science, Mansoura University, Mansoura, Egypt, for his continuous encouragement and cooperation.

References

[1] M. Kamal, A.Abdel-Salam, J.C.Pieri, J.Mater.Sci. 19, 3880-3886 (1984).

[2] Chen SW, Chen CC, Gierlotka W,Zi AR, Chen PY, Wu HJ. J.Electron Mater 37: 992-1002 (2008).

[3] Lee C, Lin CY, Yen YW. Intermetallics, 15: 1027-1037(2007).

[4] Chen SW, Chen PY, Wang CH. J Electron. Mater, 35: 1982-1985 (2006).

[5] Frear D, Vianco P. Metall Mater Trans A 25:1509-1523(1994).

[6] Geranmayeh AR, Mahmudi R, Kangooie M. Mater Sci Eng A 528: 3967-72(2011).

[7] Mahmudi R, Geranmayeh AR, Bakherad M, Allami M. Mater Sci Eng A 457: 173-9(2007).

[8] Mahmudi R, Geranmayeh AR, Rezaee-Bazzaz A. Mater Sci. Eng. A448: 287-93(2007).

[9] R.M.Shalaby, J Alloy Compd 480, 334-339 (2009).

[10] S.K.Kang, J.Horkans, P.C.Andricacos, R.A.Carruthers, J.Cotte, M.Datta, P.Gruber, J.M.E.Harper, K.Kwietniak. C.Sambucetti, L.Shi, G.Brouillette, and D.Danovitch,: 49th electronic components and technology conference (san Diego, 1999) 283-288.

[11] Ishihara s, Tamura K. Tribol Int , 43: 935-938 (2010).

[12] moazami Goudarzi M, jenabali jahromi Sa, Nazarboland A, mater.des., 30:2283-2288 (2009).

[13] A.R.Lashin, M.Mossa, A.El-Bediwi and M.Kamal, Materials and design, 43, 322-326 (2013).

[14] J.W. Jang, P.G. Kim, K.N. Tu and M. Lee: *J. Mater.Res.,* , 14(10), 3895 (1999).

[15] M.M. El-Bahay, M.E. El Mossalamy, M. Mahdy and A.A. Bahgat: *Phys. Status Solidi A,* 198(1), 76 *(*2003).

[16] K.L. Murty, M.D. Mathew and F.M. Haggag: *Met. Mater. Int.,* 4, 799 *(*1998).

[17] R.K. Mahidhara, S.M.L. Sastry, K.L. Jerina, I.Turlik and K.L. Murty: *J. Mater. Sci. Lett.,* 13(19), 1387 *(*1994).

[18] M.H.N. Beshai, S.K. Habib, A.M. Yassein, G. Saad and M.M.H. El-Naby: *Cryst. Res. Technol.,* , 34(1), 119 *(*1999).

[19] A. Yassin, R.L. Reuben, G. Saad, M.H.N. Beshai and S.K. Habib: *Proc. IME J. Mater. Des. Appl*, 213(L1), 59 *(*1999).

[20] M.Kamal, A.M.Shaban, M.El-Kady and R.M.Shalaby, Radiation Effects and Defects Solids, 138 (1996) 307.

[21] T.El-Ashram and R.M.Shalaby , Electron. Mater. 34, (2005) 212.

[22] Pecharsky Vitalij K, Zavalij Peter Y., Springer Science + Business Media, Inc.;. P. 136. (2005).

[23] B.D.Cullity, “Elements of X-ray Diffraction” 2nd, Edn (USA,1959) ch.10,p.317.

[24] K.Balakrishan, B.Vengatesan, N.Kanniah, P.Ramasamy, J.Mater.Sci. Lett. 9, 785 (1990).

[25] R.M. Shalaby, J Alloy Compd, 480**,** (2009) 334.